J Membrane Biol (2011) 239:73–84
DOI 10.1007/s00232-010-9329-3

Water Pathways in the Bacteriorhodopsin Proton Pump

Ana-Nicoleta Bondar · Stefan Fischer · Jeremy C. Smith

Received: 8 October 2010 / Accepted: 5 November 2010 / Published online: 28 November 2010

Abstract Internal water molecules play key roles in the functioning of the light-driven bacteriorhodopsin proton pump. Of particular importance is whether during the proton-pumping cycle the critical water molecule w402 can relocate from the extracellular to the cytoplasmic side of the retinal Schiff base. Here, classical mechanical and combined quantum mechanical/molecular mechanical reaction path computations are performed to investigate pathways and energetic factors influencing w402 relocation. Hydrogen bonding between w402 and the negatively charged Asp85 and Asp212 largely opposes repositioning of the water molecule. In contrast, favorable contributions from hydrogen bonding of w402 with the Schiff base and Thr89 and from the untwisting of the retinal polyene chain lower the energetic cost for water relocation. The delicate balance between the competing contributions underlies the need for highly accurate calculations and structural information.

Keywords Water · Proton transfer · Bacteriorhodopsin · QM/MM · Reaction path computation

A.-N. Bondar (✉)
Department of Physiology and Biophysics, Medical Science I, University of California at Irvine, Irvine, CA 92697-4560, USA
e-mail: nicoleta.bondar@uci.edu

A.-N. Bondar · J. C. Smith
Computational Molecular Biophysics, IWR, University of Heidelberg, 69120 Heidelberg, Germany

A.-N. Bondar
Molecular Biophysics Department, German Cancer Research Center, Im Neuenheimer Feld 580, 69120 Heidelberg, Germany

S. Fischer
Computational Biochemistry IWR, University of Heidelberg, 69120 Heidelberg, Germany

J. C. Smith (✉)
University of Tennessee/Oak Ridge National Laboratory Center for Molecular Biophysics, PO Box 2008 MS6164, Oak Ridge, TN 37831-6164, USA
e-mail: smithjc@ornl.gov

Present Address:
A.-N. Bondar
Department of Physics, Freie Universität Berlin, Arnimallee 14, 14195 Berlin, Germany

Proton pump proteins couple an energy-yielding chemical reaction—e.g., hydrolysis of adenosine triphosphate—to the uphill transport of protons across cellular membranes. The electrochemical gradient built up by a proton pump is used by the cell in processes such as the acidification of intracellular organelles (Mellman 1992) and control of the intracellular calcium concentration (Camello et al. 2000). The critical roles of proton pumps in biological cells make them valuable drug targets (Mefford and Wade 2009; Mullin et al. 2009), with inhibitors of proton pumps being "the second most commonly prescribed drug class in the United States" (Mullin et al. 2009).

The pumping of the proton across the thickness of the membrane (~37 Å; Wiener and White 1992) usually occurs in several conformation-coupled proton-transfer steps. Both amino acid side chains and internal water molecules can participate in the proton transfers. Controlled relocation of discrete water molecules at specific steps in the proton-pumping cycle may be part of the structural changes associated with proton pumping. The availability of detailed experimental observations make the light-driven bacteriorhodopsin proton pump an excellent model system to investigate the structural and energetic determinants of pathways for water relocation.

Bacteriorhodopsin is a seven-helical membrane protein that has a retinal chromophore covalently bound to Lys216 on helix G (Fig. 1a). Absorption of light by the retinal chromophore triggers isomerization of the retinal from the all-trans bR resting state configuration to 13-cis in the K state, followed by five consecutive conformation-coupled proton transfer steps that result in the net transfer of one proton from the cytoplasmic to the extracellular side of the membrane. The first proton transfer step occurs during the L-to-M transition of the reaction cycle and involves the transfer of the proton from the retinal Schiff base to the nearby Asp85 (Fig. 1a).

The high-resolution crystal structures have identified discrete water molecules present in the inter-helical cavities (Fig. 1a, b). Key functional roles of the internal water molecules have been indicated by experiments and computations (e.g., Bajaj et al. 2009; Bondar et al. 2008; Garczarek and Gerwert 2006; Gat and Sheves 1993; Hayashi and Ohmine 2000, Herzfeld and Lansing 2002; Hildebrandt and Stockburger 1984; Kandori 2004; Kouyama et al. 2004; Luecke et al. 1999; Maeda et al. 2003; Murata et al. 2000; Phatak et al. 2009). For example, internal water molecules influence the relative orientation of the proton donor and acceptor groups (Bondar et al. 2008; Gat and Sheves 1993), and can participate in storing (Garczarek and Gerwert 2006) and transferring a proton (Bondar et al. 2008; Hayashi and Ohmine 2000; Phatak et al. 2009). Of particular importance is w402, which in the bR resting state hydrogen bonds with the positively charged retinal Schiff base and the negatively charged Asp85 and Asp212 (Fig. 1a) (Nina et al. 1995; Luecke et al. 1999; Belrhali et al. 1999).

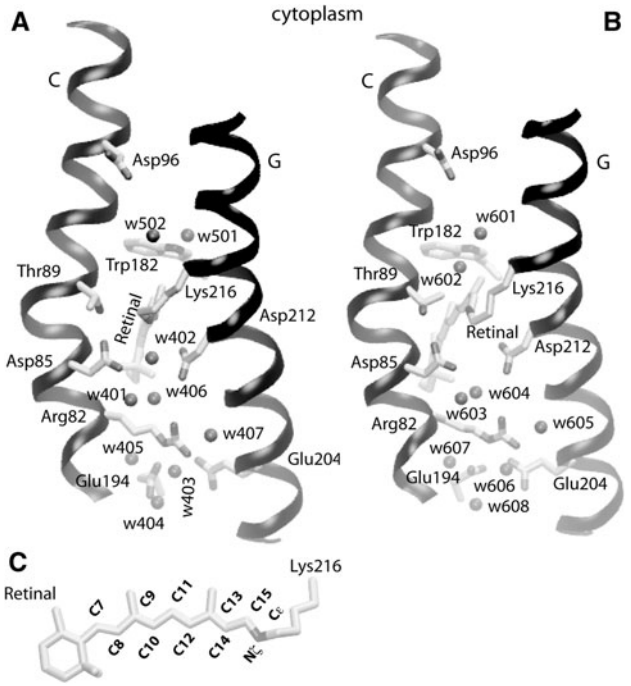

Fig. 1 Internal water molecules of bacteriorhodopsin. **a** Close view of retinal, selected amino acids and internal water molecules indicated by the crystal structure of the bR resting state (Luecke et al. 1999). The oxygen atom of the critical water molecule w402 is within hydrogen-bonding distance of the Schiff base nitrogen atom (2.9 Å) and the carboxyl oxygen atoms of Asp85 and Asp212 (2.6 and 2.8 Å, respectively). For simplicity, only helices *C* and *G* are shown. **b** Close view of retinal, selected amino acids and internal water molecules indicated by the L-state crystal structure from (Kouyama et al. 2004). The Schiff base of the 13-cis retinal points towards the cytoplasmic side, and no water molecule is present in the space occupied by w402 in the bR resting state (**a**). The distance between the Schiff base nitrogen atom and the oxygen atom of w602 is 3.3 Å. Note that the *gauche* geometry of Thr89 (rather than the *trans* geometry indicated by the crystal structure in (**b**)) is energetically favored, because it allows optimization of hydrogen bonding of the retinal Schiff base, w602, Thr89, and Asp85 (Bondar et al. 2008). (**c**) The retinal molecule and Lys216 in the crystal structure of (Luecke et al. 1999)

The crystal structures of the pre-proton-transfer state L provided conflicting information on the exact location of w402. The location corresponding to w402 in the bR resting state is occupied by a water molecule in the crystal structures from (Lanyi and Schobert 2003, 2007), but not in the crystal structures from (Edman et al. 1999, 2004; Royant et al. 2000; Kouyama et al. 2004). The absence in L of a water molecule in the location occupied by w402 in the bR resting state was suggested as due to w402 having relocated towards the extracellular side (Edman et al. 1999; Royant et al. 2000), or to the cytoplasmic side of the retinal Schiff base (Kouyama et al. 2004). Electron densities of a set of cryo-trapped K, L, and M intermediate states were interpreted as suggesting that during the K-to-L transition w402 moves from the extracellular to the cytoplasmic side of the retinal Schiff base (w602 in Fig. 1b), and that the retinal Schiff base reorients towards the cytoplasmic side of the membrane (Fig. 1b). This movement of the water molecule towards the cytoplasmic side would continue in M, rendering bacteriorhodopsin an inward water pump/outward proton pump (Kouyama et al. 2004). It has been noted (Kouyama et al. 2004) that the idea that bacteriorhodopsin could be transporting a proton outside the cell and a water molecule inside the cell is similar, albeit not identical, to the hydroxyl ion model of (Luecke et al. 2000); this model, proposed based largely on the analysis of crystal structures of bacteriorhodopsin intermediate states and considerations of the functioning of bacteriorhodopsin and the halorhodopsin chloride pump, postulates that bacteriorhodopsin may function as a net hydroxide pump (Luecke 2000; Luecke et al. 2000). Observations from nuclear magnetic resonance (NMR) experiments that in L the twisted retinal Schiff base interacts strongly with its counterion, which could be a highly polarized water molecule (Bajaj et al. 2009; Herzfeld and Lansing 2002; Mak-Jurkauskas et al. 2008), led to the question of whether bacteriorhodopsin may act as an inward hydroxyl pump, rather than an outward proton pump (Herzfeld and Lansing 2002).

Free energy computations on pre-proton transfer state L-like conformers with a cytoplasmic-oriented retinal Schiff base indicated that the pocket on the cytoplasmic side of the retinal Schiff base (Fig. 1a, b) provides an energetically favorable environment in which a water molecule is stable (Bondar et al. 2008). The free energy for inserting a water molecule in the cavity on the cytoplasmic side of the retinal Schiff base is approximately −17 kcal/mol at 150 K, and −12 kcal/mol at 300 K, arising largely from electrostatic interactions.

Whether or not w402 could relocate to the cytoplasmic side of the Schiff base will depend not only on the free energy of w402 in different positions in the bR, K, and L states, but also on the kinetic accessibility of hydration sites on the lifetimes of the K and L states. Here, we performed classical mechanical and combined quantum mechanical/molecular mechanical (QM/MM) computations to assess the energetic cost for the translocation of w402 from the extracellular to the cytoplasmic side of the retinal Schiff base. The results indicate that hydrogen bonding with Asp85 and Asp212 stabilizes w402 on the extracellular side of the retinal, and opposes its translocation towards the cytoplasmic side. Hydrogen bonding between w402 and the Schiff base and untwisting of the retinal have the opposite effect, assisting the movement of w402.

Methods

Protein Structure

Experiments indicate that the protein conformational changes in the first half of the reaction cycle are small (Bullough and Henderson 1999; Hendrikson et al. 1998; Subramaniam et al. 1999). Indeed, the crystal structures proposed for the K, L, and early M intermediates do not indicate any significant protein conformational changes relative to the bR resting state (Edman et al. 1999; Kouyama et al. 2004; Lanyi and Schobert 2003; Luecke et al. 1999; Matsui et al. 2002; Royant et al. 2000; Schobert et al. 2002). These crystal structures differ mainly in the geometrical details of the retinal Schiff base, water and protein groups close to the Schiff base.

The retinal Schiff base points towards the cytoplasmic side in (Edman et al. 1999, 2004; Kouyama et al. 2004; Royant et al. 2000), and towards the extracellular side in (Lanyi and Schobert 2003, 2007). Recent Dynamic Nuclear Polarization-Enhanced (DNP) solid-state NMR experiments revealed that at low temperatures (<170 K) there are four discrete L substates, and a single, functional L, persists upon increasing the temperature; the functional L intermediate is characterized by a strong interaction between the protonated retinal Schiff base and its counterion (Bajaj et al. 2009).

We have performed systematic computations of proton transfer and retinal configurational changes in the first half of the reaction cycle using different crystal structures (Edman et al. 1999; Lanyi and Schobert 2002, 2003, 2007; Luecke et al. 1999; Royant et al. 2000; Sass et al. 2000; Schobert et al. 2002); these computations indicate that, prior to the first proton-transfer step, a cytoplasmic-oriented conformer is likely to accumulate (Bondar et al. 2004a, 2006). For the computations reported here we used as starting coordinates the crystal structure from (Edman et al. 1999) and included water molecule w402.

The protein was capped with the neutral groups–CO–CH_3 and–NH–CH_3 added to the N (Thr5) and C (Gly231) termini, respectively. Standard protonation states were assigned to all titratable residues (i.e., acidic groups are negatively charged, and basic groups are positively charged), except for Asp115, Asp96, and Glu204, which were modeled as follows. Asp96 and Asp115 were protonated, according to the observations from experiments (Metz et al. 1992). The exact identity of the extracellular group that releases a proton to the extracellular side during the decay of the M intermediate (the proton release group) has been controversial. Earlier experiments indicated Glu204 (Fig. 1a) as the proton release group (Brown et al. 1995), or as the group that delivers the proton to Glu194 (Dioumaev et al. 1998; Kalaidzidis et al. 1998). The Glu194/Glu204 dyad, probably associated with water molecules, had also been proposed as the extracellular proton release group (Essen et al. 1998; Zscherp et al. 1999). More recent experiments suggested that the proton released to the extracellular side originated from a cluster of water molecules that interacts with protein amino acid side chains (Garczarek et al. 2005; Garczarek and Gerwert 2006). QM/MM computations of IR spectral fingerprints (Phatak et al. 2008) bring support to the proposal from experiments (Essen et al. 1998; Zscherp et al. 1999) that Glu194/Glu204, probably in association with water molecules, share the proton released to the extracellular side. In the computations presented here we modeled the protonated state of the proton release group by considering Glu204 as protonated. Test computations on the bR resting state indicate that the crystal-structure distance between Glu194 and Glu204 is well preserved when Glu204 is protonated (Bondar and Smith 2009).

In all calculations, part of the protein was flexible while the remaining protein groups were fixed to their coordinates from the crystal structure. The mobile region (827 atoms) consisted of the retinal, one layer of surrounding residues, and water molecules and protein groups whose coordinates were considered as likely to change as a result of the structural rearrangements in the active site.

Potential Energy Function

Computations were performed using the MM or the QM/MM description. The interactions between the classical (MM) atoms are given by the CHARMM (Chemistry at HARvard Macromolecular Mechanics) potential energy function (Brooks et al. 1983) and grouped here as

$$E = E_{bonded} + E_{non-bonded}, \quad (1)$$

where E is the total energy of the system, the bonded energy is the sum of the bond stretching, angle bending, dihedral angle torsions, out-of-plane deformations, and Urey-Bradley 1:3 interactions, and the nonbonded interactions are the sum of the Coulomb and van der Waals interactions (Brooks et al. 1983).

In the QM/MM approach, the active site of the protein is described with QM, whereas the rest of the protein environment is treated with MM (Field et al. 1990; Singh and Kollman 1986; Warshel 1991). For the QM/MM computations, the protein was partitioned into QM and MM regions using the link-atom approach to satisfy the empty valence at the QM host (Field et al. 1990). In all QM/MM refinements, the QM region included the retinal, the side chains of Lys216, Asp85, Thr89, and Asp212, and w402 (86 atoms); w401 and w406 were also included in the QM/MM-refined paths reported here. Link atoms were attached to C_β of Lys216 and to C_α of Asp85, Thr89, and Asp212.

Interactions between MM atoms were computed using the hybrid description of the protein amino acid side chains in which the all-atom (MacKerell et al. 1998) and extended atom representations (Neria et al. 1996) are used for the aromatic side chains and for the aliphatic groups, respectively. In the MM computations, the retinal was described using the parameter set from (Nina et al. 1995) that accounts for the interaction between the Schiff base and water. MM water molecules were described with TIP3P (Jorgensen et al. 1983). The relative dielectric constant was set to one. The interactions between the QM and MM parts of the system were computed using the self-consistent charge density functional tight-binding approach (SCC-DFTB) (Cui et al. 2001; Elstner et al. 1998) to describe the QM atoms. SCC-DFTB provides a good description of the retinal structural properties (Zhou et al. 2002) and proton transfer energetics (Bondar et al. 2004a, b, 2007). Detailed discussions of the QM/MM description of bacteriorhodopsin and of the accuracy of SCC-DFTB for describing retinal geometry and proton transfer are given in (Bondar et al. 2007, 2010).

Reaction Pathway Calculations

Reaction paths were computed using the conjugate peak refinement (CPR) algorithm (Fischer and Karplus 1992) which allows the complex degrees of freedom involved in retinal protein function to be simultaneously varied. Starting from energy-optimized reactant and product state structures, the CPR algorithm finds a minimum-energy pathway along which the energy maxima are first-order saddle points that give the transition states of the reaction. Intermediate conformers prepared with adiabatic mapping were used in the initial paths; these intermediate states were refined along with the other intermediate path points. The CPR pathways were refined by optimizing the path points with the synchronous chain minimization algorithm (SCM) (Choi and Elber 1991) as implemented in the TRAvel (Trajectory Refinement Algorigthms) 0.42 module of CHARMM (Fischer and Karplus 1992). SCM brings the path segments between the stationary states of the path closer to the valleys of the potential energy surface. The minimum-energy pathway resulted from the CPR/SCM refinement yields the intrinsic reaction coordinate, which measures the curvilinear distance along the path.

For the computations described here, we define as the reactant (R) state the conformers in which w402 occupies its location between Asp85 and Asp212, and as the product (P) state the conformer characterized by w402 being located on the cytoplasmic side of the retinal Schiff base. The R and P conformers of all paths were energy-optimized to a RMS energy gradient of 10^{-3} kcal/mol Å. The lowest-energy local minimum and the highest-energy saddle point along the path are denoted as the LM and S conformers, respectively.

Results

We computed pathways for the movement of w402 from the extracellular to the cytoplasmic side of the retinal Schiff base on the both Thr89 and Asp212 sides of the retinal Schiff base. The path on the Thr89 side of the retinal was computed at the both MM and QM/MM levels (Table 1). The MM description of the system has the advantage of simplicity in dissecting how various structural elements contribute to the energy profile of the path. Comparing the results obtained with MM and QM/MM

Table 1 Pathways for translocation of w402 across the retinal Schiff base region

Path	Retinal side	Potential energy function	$\Delta E^{\#}$ (kcal/mol)
1	Thr89	MM	10.8
1′	Thr89	QM/MM	15.2
2	Asp212	QM/MM	13.4

$\Delta E^{\#}$ was calculated as the energy difference between the highest-energy saddle point S and the reactant state R

descriptions of the system allows us to assess how the results depend on the level of the theoretical treatment.

In what follows, we describe briefly the main results of the reaction path computations.

Pathway for Translocation of w402 on the Thr89 Side of the Retinal Computed with MM (Path **1**)

Translocation of w402 on the Thr89 side is accompanied by rearrangements of the retinal chain and the Thr89 and Asp85 side chains; in contrast, Asp212 undergoes negligible rearrangements (Fig. 2). Breaking of the hydrogen bond between w402 and Asp212 with reorientation of w402 such that it makes two hydrogen bonds with Asp85 gives the rate-limiting saddle point of the path, located at a value $\lambda = 0.28$ of the normalized reaction coordinate (see conformer S in Figs. 2b, 3a). Decomposition of the energy profile of path **1** according to Eq. 1 indicates that the energetic cost for water translocation arises from nonbonded interactions; the dihedral angle term of the bonded interactions has the opposite effect, lowering the total energy (Fig. 3a).

Inspection of the sequence of conformational changes along path **1** indicates that, as w402 moves across the lumen lined by the retinal, Thr89, and Asp85, the retinal polyene chain becomes more planar in the Schiff base segment (Figs. 2a, 3b, g). Untwisting of the retinal Schiff base segment (Figs. 2, 3b) leads to a favorable contribution from the dihedral angle term of the retinal (Fig. 3c), which explains the favorable contribution of the dihedral angle term to the total energy of path **1** (Fig. 3a).

Rearrangement of hydrogen bonds between the active-site water molecules and their protein environment makes a significant contribution to the energy profile of path **1** (Fig. 3e–g). Reorientation of w402 with both OH bonds towards Asp85 (compare R and S intermediates in Fig. 2b) is associated with unfavorable energies of interaction between w402 and Asp212 (see energy values at $\lambda = 0.28$; Fig. 3e, g). Hydrogen bonding between w402 and Asp85 brings strongly favorable contributions (on the order of -10 kcal/mol) in the segment of the path that includes the rate-limiting saddle point (Fig. 3a, e). Breaking of the w402:Asp85 hydrogen bond (Fig. 3g) upon movement of w402 to the cytoplasmic side of the retinal is energetically strongly unfavorable (Fig. 3e), but this is largely compensated by the formation of a hydrogen bond between w402 and the Schiff base (Fig. 3e, g; see also conformer P in Fig. 2b). For w402 to move across the space between Thr89 and the retinal Schiff base (Fig. 2), the Thr89:Schiff base hydrogen bond, which is present in the reactant state (Fig. 2a), must break (Fig. 3h). Breaking of the hydrogen bond leads to an increase of the Thr89:Schiff base interaction energy by 6.6 kcal/mol at the rate-limiting saddle point (Fig. 3d).

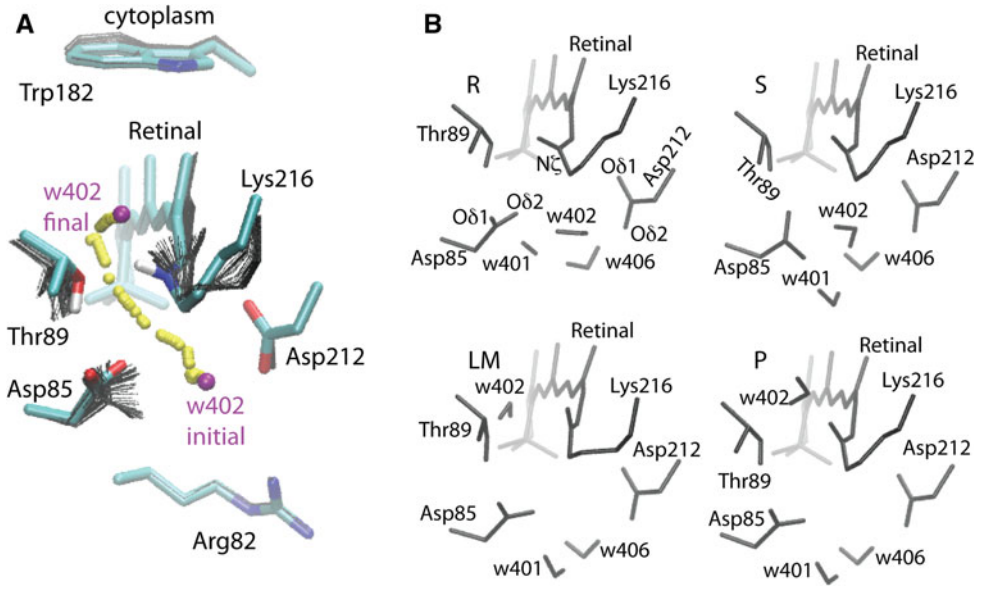

Fig. 2 Pathway for translocation of w402 on the Thr89 side of the retinal computed with MM (path **1**). **a** "Movie" of path **1** showing the locations of the w402 oxygen atom (small spheres) as it moves from the initial location on the extracellular side of the retinal Schiff base, to the final location on the cytoplasmic side of the Schiff base. Retinal and selected protein amino acids are shown as thick bonds in the initial (reactant, R) intermediate, and as thin lines for all other coordinate sets along the pathway. **b** Schematic representations of active-site geometries in the reactant (*R*), highest-energy saddle point (*S*), lowest-energy local minimum (*LM*), and product intermediate (*P*) of path **1**. The schematic representation of the R intermediate of path **1** also indicates the retinal and protein atom names used for distance measurements in Figs. 3–5

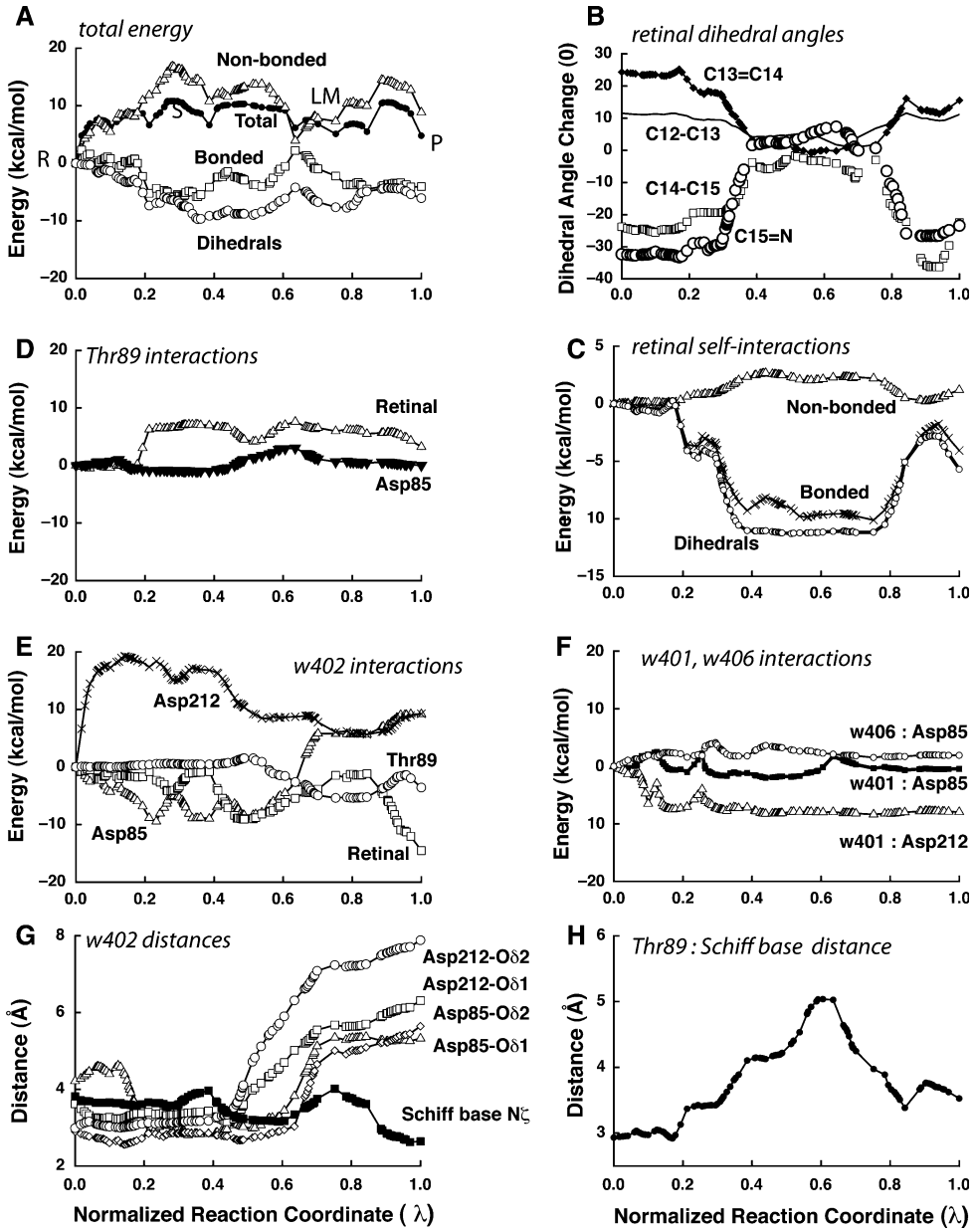

Fig. 3 Energy profile and structural changes along path **1**. The reaction coordinate λ is the sum of root-mean-squared differences in atomic coordinates, normalized to the total length of the path (Fischer and Karplus 1992). All energies are MM-optimized values (kcal/mol) taken relative to the R state at $\lambda = 0$. Water molecule w402 is located on the extracellular side of the retinal Schiff base at $\lambda = 0$, and on the cytoplasmic side at $\lambda = 1$. **a** Energy profile of path **1**. The R, S, LM, and P intermediates are at λ values of 0.00, 0.28, 0.75, and 1.00, respectively (see also Fig. 2b). The total energy profile, shown as *solid circles,* is decomposed into the bonded (*open squares*) and nonbonded terms (*open triangles*) (see discussion of Eq. 1 in "Methods" section). The dihedral angle contribution to the total bonded energy is depicted as *open circles.* **b** Translocation of w402 in path **1** is accompanied by significant changes in the retinal angles. All retinal dihedral angles are in degrees. The value of the C_{12}–$C_{13} = C_{14}$–C_{15} measured along path **1** (*solid diamonds*) is compared to the values of the $C_{11} = C_{12}$–$C_{13} = C_{14}$ (*continuous line*), $C_{13} = C_{14}$–$C_{15} = N$ (*open squares*), and C_{14}–$C_{15} = N$–Cε dihedral angles (*open circles*) taken relative to the value in the reactant state R. The reactant-state values of the $C_{11} = C_{12}$–$C_{13} = C_{14}$, $C_{13} = C_{14}$–$C_{15} = N$, and C_{14}–$C_{15} = N$–Cε dihedral angles are 168.5, −156.2, and −147.7 degrees, respectively. See Fig. 1c for the numbering of retinal atoms. **c** Untwisting of the retinal polyene chain contributes to lowering the energy for water translocation in path **1**. **d** Nonbonded interactions between Thr89 and the retinal (*open squares*), and between Thr89 and Asp85 (*solid triangles*). **e** Nonbonded interaction energies between w402, retinal, and selected protein amino acids. The repulsive interactions between w402 and Asp212 largely contribute to the rate-limiting energy barrier, whereas the favorable interactions of w402 with Asp85, the Schiff base, and Thr89, assist water translocation. See Fig. 2 for snapshots of w402 locations. **f** Nonbonded interactions between w401 and Asp85 (*solid squares*), w402 and Asp212 (*open triangles*), and between w406 and Asp85 (*open circles*). **g** Distances (Å) between the w402 oxygen atom and selected retinal and protein atoms measured along path **1**. **h** Distance (Å) between the hydroxyl oxygen atom of Thr89 and the Schiff base nitrogen

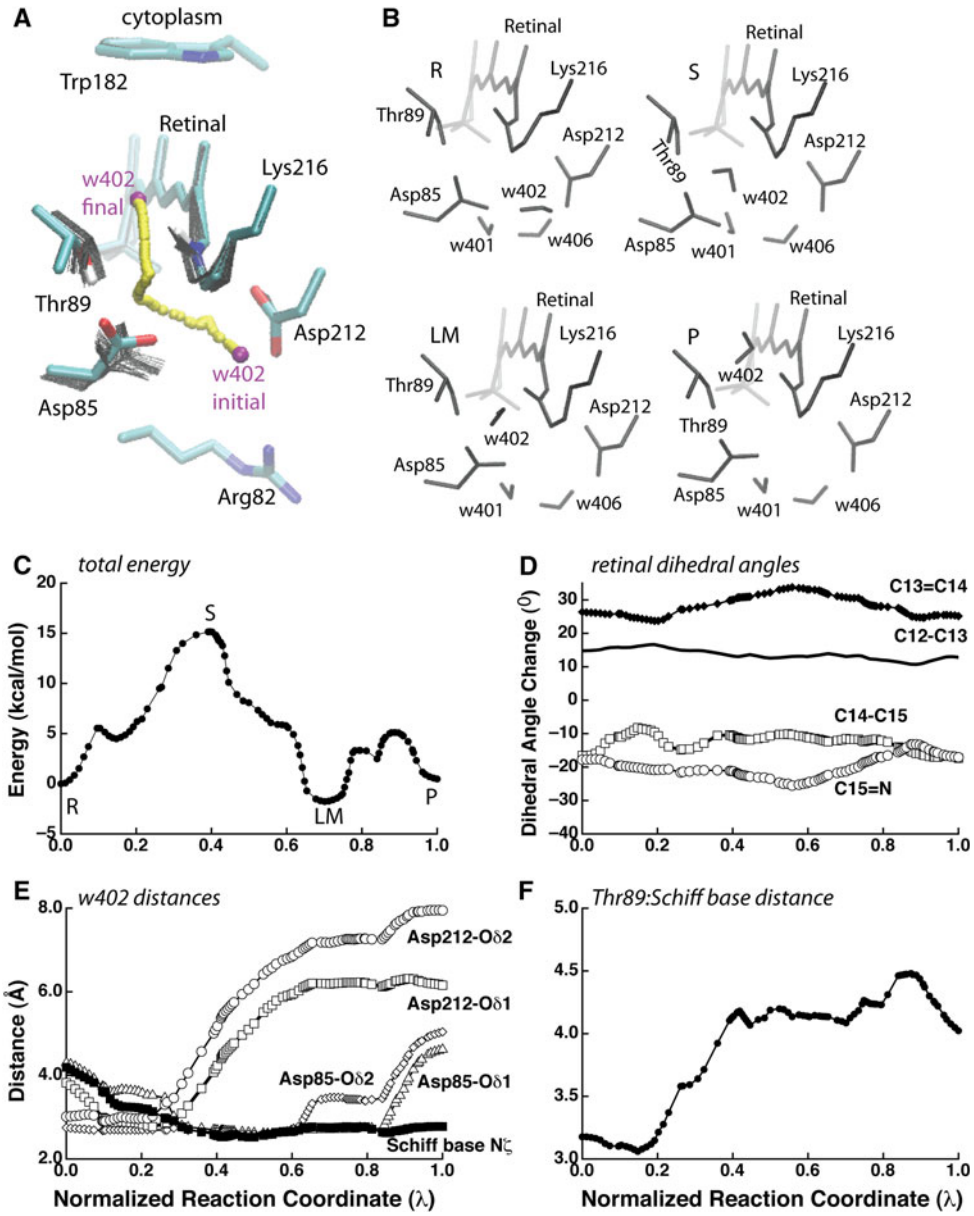

Fig. 4 QM/MM pathway for translocation of w402 on the Thr89 side of the retinal (path **1′**). **a** "Movie" of path **1′** showing the locations of the w402 oxygen atom as small spheres, retinal and selected protein amino acids as thick bonds in the R state, and as thin lines for all other configurations sampled along the pathway. **b** Schematic representations of active-site geometries in the *R*, *S*, *LM*, and *P* intermediates of path **1′**, located at λ values of 0.00, 0.4, 0.7, and 1.00, respectively (see **c**). The distance between the Thr89 hydroxyl oxygen atom and the Schiff base nitrogen increases from 3.2 Å in the R state to 4.1 Å in *S*. **c** Energy profile of path **1′. d** Changes of selected retinal dihedral angles along path **1′** measured as detailed in Fig. 3b. Note the much smaller variations of the retinal dihedral angles in path **1′** than in path **1** (compare Fig. 3b with (**d**), and Fig. 2a with (**a**)). **e** Distances between the w402 oxygen atom and selected retinal and protein atoms measured along path **1′. f** Distance between the hydroxyl oxygen atom of Thr89 and the Schiff base nitrogen. The hydrogen bond between Thr89 and the Schiff base, which is present at the beginning of the pathway, breaks as w402 relocates to the cytoplasmic side (see also (**e**)). A collection of movies pertaining to proton transfer paths in bacteriorhodopsin can be found at http://www.iwr.uni-heidelberg.de/groups/biocomp/fischer

Pathway for Translocation of w402 on the Thr89 Side of the Retinal Computed with QM/MM (Path **1′**)

Previous computations indicated that details of hydrogen bonding in the active site of retinal proteins can depend on the theoretical level used to describe the retinal: the strength of the hydrogen bond between the Schiff base and Thr89 is underestimated when bacteriorhodopsin is described with SCC-DFTB/MM, as compared to B3LYP 6-31G**/MM (Bondar et al. 2007), and the parameters

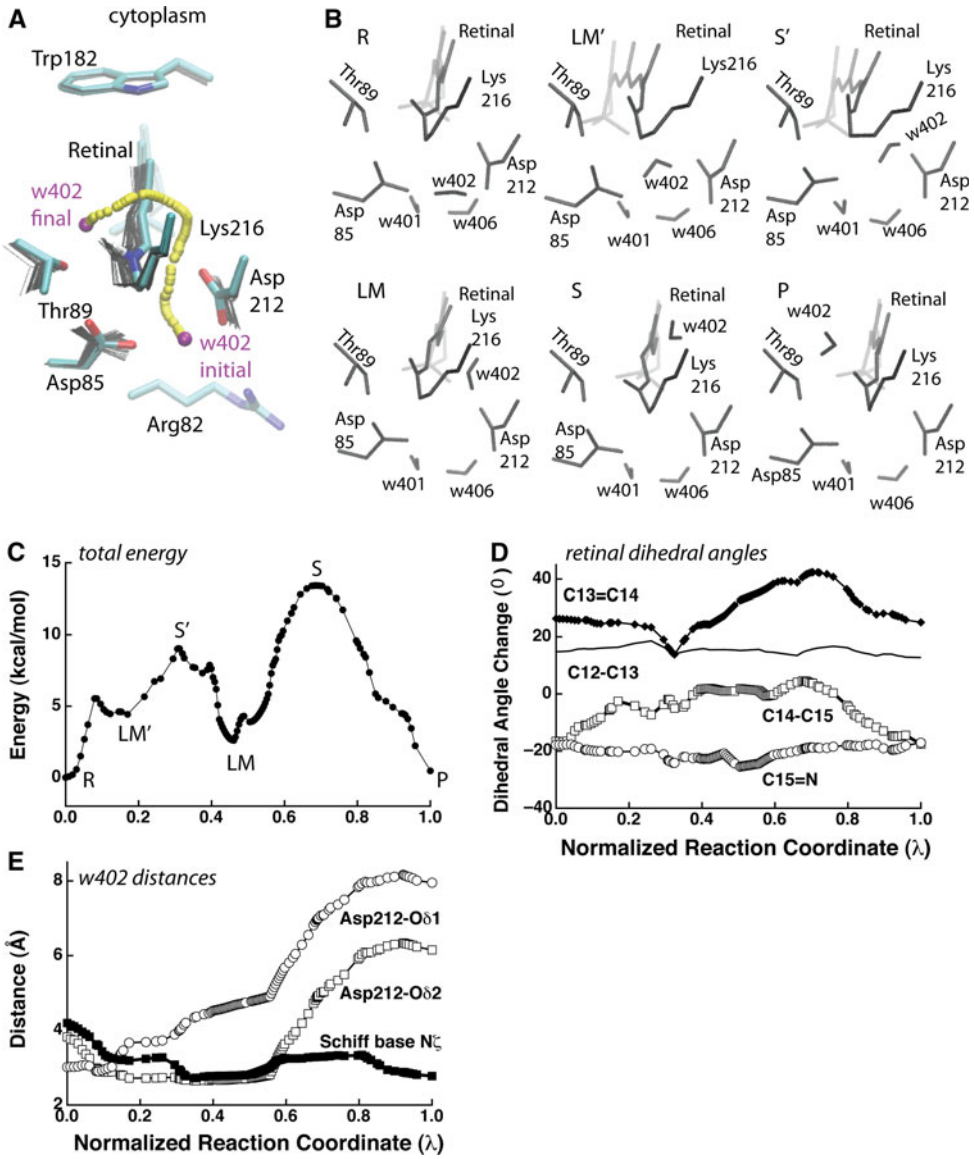

Fig. 5 QM/MM pathway for translocation of w402 on the Asp212 side of the retinal (path **2**). **a** Pathway followed by the oxygen atom of w402, depicted as in Figs. 2a and 4a. **b** Schematic representations of active-site geometries in the *R*, *LM*′, *S*′, *LM*, *S*, and *P* intermediates of path **2**, which are found at λ values of 0.00, 0.17, 0.31, 0.46, 0.69, and 1.00, respectively. The *S*′ and *LM*′ intermediates represent the second highest saddle point and the second lowest energy minimum, respectively. **c** Energy profile of path **2′.** **d** Changes of selected retinal dihedral angles along path **2′** measured as detailed in Fig. 3b. **e** Distances between the w402 oxygen atom and selected retinal and protein atoms measured along path **2**

used to describe the retinal and its interactions with water molecules can affect the geometry and the dynamics of the retinal in its tight binding pocket environment in squid rhodopsin (Jardón-Valadez et al. 2010).

The QM/MM-optimized pathway for translocation of w402 on the Thr89 side of the retinal (path **1′**; Fig. 4) indicates similar structural rearrangements being associated with the rate-limiting barrier as in path **1**: breaking of the hydrogen bonds between w402 and Asp212, formation of two hydrogen bonds between w402 and Asp212, and an increase of the distance between the Thr89 hydroxyl group and the Schiff base (Fig. 4b, c, f). An important difference between the structural changes associated with paths **1** and **1′** is that the amplitude of the structural changes undergone by the retinal Schiff base segment is much smaller in path **1′** than in path **1** (compare Figs. 2a with 4a, and Figs. 3b with 4d). Unlike in path **1**, where translocation of w402 is assisted by the favorable energy of untwisting the Schiff base segment (Figs. 3a–c), the Schiff base segment remains twisted along path **1′** (Fig. 4d). The absence of favorable contributions from untwisting the retinal chain likely explains the rate-limiting barrier of path **1′** being $\sim$4 kcal/mol higher than that of path **1**.

The lowest-energy intermediate along path **1′** is the local minimum LM at $\lambda = 0.7$ (Fig. 4c), which is 1.8 kcal/mol and 2.3 kcal/mol lower in energy than the R and P conformers, respectively. The LM conformer (Fig. 4b) is characterized by w402 bridging the positively charged Schiff base and the negatively charged Asp85. LM is separated from the R conformer by the 15.2 kcal/mol

rate-limiting barrier of path **1′**, and from P by a barrier of 4.5 kcal/mol (Fig. 4c).

Pathway for Translocation of w402 on the Asp212 Side of the Retinal Computed with QM/MM (Path **2**)

Translocation of w402 on the Asp212 side of the retinal starts with relocation of w402 away from Asp85, and rearrangement of the retinal polyene chain and of the Lys216 side chain to accommodate w402 moving to the Asp212 side of the retinal (Fig. 5a, b); these structural rearrangements give saddle point S' at $\lambda = 0.31$ with an associated energy barrier of 9.0 kcal/mol (Fig. 5b, c). Further movement of w402 (Fig. 5a, b, e) leads to the strong hydrogen bonding between w402 and Asp212 (Fig. 5e) that characterizes the low-energy local minimum LM at $\lambda = 0.46$ (Fig. 5c). Movement of w402 through the hydrophobic cavity on the cytoplasmic side of the Lys216 side chain (Fig. 5a) gives the 13.4 kcal/mol rate-limiting barrier of path **2**.

The twist of the retinal Schiff base segment along path **2** is towards Thr89 (Fig. 5a, b). We did not observe hydrogen bonding between w402 and the Schiff base in the region of the path that contains the energetically unfavorable passage of w402 through the hydrophobic cavity on the Lys216 side chain (see conformer S in Fig. 5b). Test QM/MM calculations in which the retinal Schiff base was constrained to twist back towards Asp212 did not indicate a decrease in the rate-limiting barrier for water passage on the Asp212 side.

Discussion

In the bR resting state, w402 hydrogen bonds with the protonated Schiff base and the negatively charged Asp85/Asp212 (Belrhali et al. 1999; Luecke et al. 1999) (Fig. 1a). These favorable interactions between w402 and its protein environment explain the high probability of occupancy of w402 indicated by free energy computations (Baudry et al. 2001; Roux et al. 1996). The pocket on the cytoplasmic side of the retinal Schiff base could stabilize a water molecule in the both bR (Roux et al. 1996) and L-like states (Bondar et al. 2008). However, a favorable free energy for inserting a water molecule in the cavity at the cytoplasmic side of the retinal Schiff base does not necessarily mean that the cavity is occupied by water, as the presence of the water molecule in the cavity will depend on the difference between the free energies of the water in the starting and ending location, and on whether the energetic barrier for water relocation can be overcome on the timescale of the reaction cycle.

The computations presented here indicate that breaking of the favorable interactions between w402 and Asp212, and increasing the distance between Thr89 and the Schiff base, both oppose translocation of w402 on the Thr89 side of the retinal (path **1**; Fig. 3d, e). In contrast, translocation of w402 to the cytoplasmic side of the retinal Schiff base is assisted by hydrogen bonding between Asp85 and w402, and by the formation of a hydrogen bond between the Schiff base and w402 upon translocation of w402 (Figs. 2–4).

Translocation of w402 on the Thr89 side of the retinal could also be facilitated by untwisting of the retinal chain (Fig. 3a–c). We find that the magnitude of the conformational changes in the retinal Schiff base segment along the path for translocation of w402 on the Thr89 side of the retinal depends on the theoretical level used to describe the retinal (compare Figs. 2a, 4a, and 3b, 4d). Retinal can twist relatively easily (Fig. 2a) when described with the MM force-field parameter set of (Nina et al. 1995), in which Hartree-Fock computations were used to derive the barriers for retinal dihedral angle torsions. In contrast, smaller structural rearrangements are observed when retinal is described with SCC-DFTB (path **1′**; Fig. 3a). The absence of the favorable energetic contributions from untwisting of the retinal polyene chain likely accounts for the rate-limiting barrier for water translocation being $\sim$5 kcal/mol higher when computed with SCC-DFTB than with the force field from (Nina et al. 1995).

At the QM/MM level, the rate-limiting barrier for the translocation of w402 is $\sim$2 kcal/mol smaller on the Asp212 side of the retinal (path **2**; 13.4 kcal/mol) than on the Thr89 side (path **1′**; 15.2 kcal/mol). The rate-limiting barrier for translocation of w402 on the Asp212 side of the retinal is associated with the movement of w402 across the hydrophobic region on the cytoplasmic side of the Lys216 side chain (Fig. 5).

The relatively large energy barriers for water translocation found here, around 10–15 kcal/mol, likely explain why no water molecules were found to diffuse across the Schiff base segment on the nanosecond timescale in previous molecular dynamics simulations on the bR and M intermediate states (Grudinin et al. 2005).

The lowest-energy conformer along the QM/MM path for the translocation of w402 on the Thr89 side of the retinal (path **1**; Fig. 2) is characterized by the protonated retinal Schiff base and the negatively charged Asp85 being bridged via hydrogen bonding with w402 (see conformer LM in Fig. 4b). This low-energy conformer is separated by energy barriers of 15.2 kcal/mol and 4.5 kcal/mol from conformers in which w402 is on the extracellular and the cytoplasmic side, respectively. In QM/MM molecular dynamics at 300 K performed in the presence of a water molecule on the cytoplasmic side of the retinal Schiff base and in the absence of a water molecule at position w402 (i.e., as indicated by the crystal structure of Kouyama et al. 2004; see Fig. 1b), we observed that the cytoplasmic water

molecule relocates so as to bridge the retinal Schiff base and the negatively charged Asp85 (Bondar et al. 2008); the presence of this bridge is consistent with NMR data (Bajaj et al. 2009). The QM/MM reaction path computations and molecular dynamics simulations would suggest that the low-energy conformer in which w402 bridges the Schiff base with Asp85 (conformer LM in Fig. 4b) may be reached more easily by a water molecule leaving from the cytoplasmic side than from the extracellular side. The cytoplasmic water molecule could originate from the relocation of weakly binding water molecules on the cytoplasmic side of the retinal Schiff base indicated by spectroscopy (Maeda et al. 2003).

The magnitude of the rate-limiting energy barriers for the translocation of w402 across the retinal Schiff base region is compatible with the millisecond kinetics of the bacteriorhodopsin reaction cycle. However, our finding that untwisting of the retinal chain could be a critical determinant of the energetics of water translocation suggests that more studies are necessary in order to conclude definitively whether translocation of w402 can occur, and at what step during the reaction cycle. Higher-level QM methods for describing the retinal chain and highly accurate experimental information on the geometry of the 13-cis retinal would be required.

Acknowledgments This work was financed in part by the Deutsche Forschungsgemeinschaft (SM 63/7). ANB was supported by grants GM74637 and GM-86685 from the National Institutes of General Medical Sciences. JCS was supported by a Laboratory-Directed Research and Development grant in Systems Biology to Oak Ridge National Laboratory from the U.S. Department of Energy.

Reference

Bajaj VS, Mak-Jurkauskas ML, Belenky M, Herzfeld J, Griffin RG (2009) Functional and shunt states of bacteriorhodopsin resolved by 250 GHz dynamic nuclear polarization-enhanced solid-state NMR. Proc Natl Acad Sci USA 106:9244–9249

Baudry J, Tajkhorshid E, Molnar E, Phillips J, Schulten K (2001) Molecular dynamics study of bacteriorhodopsin and the purple membrane. J Phys Chem B 105:905–918

Belrhali H, Nollert P, Royant A, Menzel C, Rosenbuch JP, Landau EM, Pebay-Peyroula E (1999) Protein, lipid and water organization in bacteriorhodopsin crystals: a molecular view of the purple membrane at 1.9 Å resolution. Structure 7:909–917

Bondar AN, Smith JC (2009) Water molecules in short- and long-distance proton transfer steps of bacteriorhodopsin proton pumping. Isr J Chem 48:155–161

Bondar AN, Elstner M, Suhai S, Smith JC, Fischer S (2004a) Mechanism of primary proton transfer in bacteriorhodopsin. Structure 12:1281–1288

Bondar AN, Fischer S, Smith JC, Elstner M, Suhai S (2004b) Key role of electrostatic interactions in bacteriorhodopsin proton transfer. J Am Chem Soc 126:14668–14677

Bondar AN, Smith JC, Fischer S (2006) Structural and energetic determinants of primary proton transfer in bacteriorhodopsin. Photochem Photobiol Sci 5:547–552

Bondar AN, Suhai S, Fischer S, Smith JC, Elstner M (2007) Suppression of the back proton-transfer from Asp85 to the retinal Schiff base in bacteriorhodopsin: a theoretical analysis of structural elements. J Struct Biol 157:454–469

Bondar AN, Baudry J, Suhai S, Fischer S, Smith JC (2008) Key role of water molecules in bacteriorhodopsin proton transfer reactions. J Phys Chem B 112:14729–14741

Bondar AN, Smith JC, Elstner M (2010) Mechanism of a proton pump analyzed with computer simulations. Theor Chem Acc 125:353–363

Brooks BR, Bruccoleri RE, Olafson BD, States DJ, Swaminathan S, Karplus M (1983) CHARMM: a program for macromolecular energy, minimization, and dynamics calculations. J Comput Chem 4:187–217

Brown LS, Sasaki J, Kandori H, Maeda A, Needleman R, Lanyi JK (1995) Glutamic acid 204 is the terminal proton release group at the extracellular surface of bacteriorhodopsin. J Biol Chem 270:27122–27126

Bullough PA, Henderson R (1999) The projection structure of the low temperature K intermediate of the bacteriorhodopsin photocycle determined by electron diffraction. J Mol Biol 286:1663–1671

Camello C, Pariente JA, Salido GM, Camello PJ (2000) Role of proton gradients and vacuolar H^+-ATPases in the refilling of intracellular calcium stores in exocrine cells. Curr Biol 10:161–164

Choi C, Elber R (1991) Reaction path study of helix formation in tetrapeptides: effect of sidechains. J Chem Phys 94:751–760

Cui Q, Elstner M, Kaxiras E, Frauenheim T, Karplus M (2001) A QM/MM implementation of the self-consistent charge density functional tight binding (SCC-DFTB) method. J Phys Chem B 105:569–585

Dioumaev A, Richter H-T, Brown LS, Tanio M, Tuzi S, Saito H, Kimura Y, Needleman R, Lanyi JK (1998) Existence of a proton transfer chain in bacteriorhodopsin: participation of Glu-194 in the release of protons to the extracellular surface. Biochem 37:2496–2506

Edman K, Nollert P, Royant A, Belrhali H, Pebay-Peyroula E, Hajdu J, Neutze R, Landau EM (1999) High-resolution X-ray structure of an early intermediate in the bacteriorhodopsin photocycle. Nature 401:822–826

Edman K, Royant A, Larsson G, Jacobson F, Taylor T, van der Spoel D, Landau EM, Pebay-Peyroula E, Neutze R (2004) Deformation of helix C in the low temperature L-intermediate of bacteriorhodopsin. J Biol Chem 279:2147–2158

Elstner M, Porezag D, Jungnickel G, Elsner J, Haugk M, Frauenheim T, Suhai S, Seifert G (1998) Self-consistent-charge-density-functional tight-binding method for simulations of complex material properties. Phys Rev B 58:7260–7268

Essen LO, Siegert R, Lehman WD, Oesterhelt D (1998) Lipid patches in membrane protein oligomers: crystal structure of the bacteriorhodopsin–lipid complex. Proc Natl Acad Sci USA 95: 11673–11678

Field MJ, Bash PA, Karplus M (1990) A combined quantum mechanical and molecular mechanical potential for molecular dynamics. J Comput Chem 11:700–733

Fischer S, Karplus M (1992) Conjugate peak refinement: an algorithm for finding reaction paths and accurate transition states in systems with many degrees of freedom. Chem Phys Lett 194:252–261

Garczarek F, Gerwert K (2006) Functional waters in intraprotein proton transfer monitored by FTIR difference spectroscopy. Nature 439:109–112

Garczarek F, Brown LS, Lanyi JK, Gerwert K (2005) Proton binding within a membrane protein by a protonated water cluster. Proc Natl Acad Sci USA 102:3633–3638

Gat Y, Sheves M (1993) A mechanism for controlling the pKa of the retinal protonated Schiff base in retinal proteins. A study with model compounds. J Am Chem Soc 115:3772–3773

Grudinin S, Büldt G, Gordeliy V, Baumgartner A (2005) Water molecules and hydrogen-bonded networks in bacteriorhodopsin—molecular dynamics simulations of the ground state and the M-intermediate. Biophys J 88:3252–3261

Hayashi S, Ohmine I (2000) Proton transfer in bacteriorhodopsin: structure, excitation, IR spectra, and potential energy surface analyses by an ab initio QM/MM method. J Phys Chem B 104:10678–10691

Hendrikson FM, Burkard F, Glaeser RM (1998) Structural characterization of the L-to-M transition of the bacteriorhodopsin photocycle. Biophys J 75:1446–1454

Herzfeld J, Lansing JC (2002) Magnetic resonance studies of the bacteriorhodopsin pump cycle. Annu Rev Biophys Biomol Struct 31:73–95

Hildebrandt P, Stockburger M (1984) Role of water in bacteriorhodopsin's chromophore: resonance Raman study. Biochem 23:5539–5548

Jardón-Valadez E, Bondar AN, Tobias DJ (2010) Coupling of retinal, protein, and water dynamics in squid rhodopsin. Biophys J 99:2200–2207

Jorgensen W, Chandrasekhar J, Madura J, Impey R, Klein M (1983) Comparison of simple potentials for simulation of liquid water. J Comp Chem 79:926–935

Kalaidzidis IV, Belevich IN, Kaulen AD (1998) Photovoltage evidence that Glu-204 is the intermediate proton donor rather than the terminal proton release group in bacteriorhodopsin. FEBS Lett 434:197–200

Kandori H (2004) Hydration switch model for the proton transfer in the Schiff base region of bacteriorhodopsin. Biochim Biophys Acta 1658:72–79

Kouyama T, Nishikawa T, Tokuhisa T, Okumura H (2004) Crystal structure of the L intermediate of bacteriorhodopsin: evidence for vertical translocation of a water molecule during the proton pumping cycle. J Mol Biol 335:531–546

Lanyi JK, Schobert B (2002) Crystallographic structure of the retinal and the protein after deprotonation of the Schiff base: the switch in the bacteriorhodopsin photocycle. J Mol Biol 321:727–737

Lanyi JK, Schobert B (2003) Mechanism of proton transport in bacteriorhodopsin from crystallographic structures of the K, L, M_1, M_2, and M_2' intermediates of the photocycle. J Mol Biol 328:439–450

Lanyi JK, Schobert B (2007) Structural changes in the L photointermediate of bacteriorhodopsin. J Mol Biol 365:1379–1392

Luecke H (2000) Atomic resolution structures of bacteriorhodopsin photocycle intermediates: the role of discrete water molecules in the function of this light-driven ion pump. Biochim Biophys Acta 1460:133–156

Luecke H, Schobert B, Richter HT, Cartailler JP, Lanyi JK (1999) Structure of bacteriorhodospin at 1.55 Å resolution. J Mol Biol 291:899–911

Luecke H, Schobert B, Cartailler HTR, Rosengarth A, Needleman R, Janyi JK (2000) Coupling photoisomerization of retinal to directional transport in bacteriorhodopsin. J Mol Biol 300:1237–1255

MacKerell AD Jr, Bashford D, Bellott RL, Dunbrack RL Jr, Evanseck JD, Field MJ, Fischer S, Gao J, Guo H, Ha S, Joseph-McCarthy D, Kuchnir L, Kuczera K, Lau FTK, Mattos C, Michnick S, Ngo T, Nguyen DT, Prodhom B, Reiher WE III, Roux B, Schlenkrich M, Smith JC, Stote R, Straub J, Watanabe M, Wiorkiewicz-Kuczera J, Yin D, Karplus M (1998) All-atom empirical potential for molecular modeling and dynamics studies of proteins. J Phys Chem B 102:3586–3616

Maeda A, Herzfeld J, Belenky M, Needleman R, Gennis RB, Balashov SP, Ebrey TG (2003) Water-mediated hydrogen-bonded network on the cytoplasmic side of the Schiff base of the L photointermediate of bacteriorhodopsin. Biochemistry 42:14122–14129

Mak-Jurkauskas ML, Bajaj VS, Hornstein MK, Belenky M, Griffin RG, Herzfeld J (2008) Energy transformations early in the bacteriorhodopsin photocycle revealed by DNP-enhanced solid-state NMR. Proc Natl Acad Sci USA 105:883–888

Matsui Y, Sakai K, Murakami M, Shiro Y, Adachi S, Okumura H, Kouyama T (2002) Specific damage induced by X-ray radiation and structural changes in the primary photoreaction of bacteriorhodopsin. J Mol Biol 324:469–481

Mefford IN, Wade EU (2009) Proton pump inhibitors as a treatment method for type II diabetes. Med Hypotheses 73:29–32

Mellman I (1992) The importance of being acid: the role of acidification in intracellular membrane traffic. J Exp Biol 172:39–45

Metz G, Siebert F, Engelhard M (1992) Asp85 is the only internal aspartic acid that gets protonated in the M intermediate and the purple-to-blue transition of bacteriorhodopsin. A solid-state and ^{13}C CP-MAS NMR investigation. FEBS Lett 303:237–241

Mullin JM, Gabello M, Murray LJ, Farrel CP, Bellows J, Wolov KR, Kearney KR, Rudolph D, Thornton JJ (2009) Proton pump inhibitors: actions and reactions. Drug Discov Today 14:647–660

Murata K, Fuji Y, Enomoto N, Hata M, Hoshino T, Tsuda M (2000) A study on the mechanism of the proton transport in bacteriorhodopsin: the importance of the water molecule. Biophys J 79:982–991

Neria E, Fischer S, Karplus M (1996) Simulation of activation free energies in molecular systems. J Chem Phys 105:1902–1921

Nina M, Roux B, Smith JC (1995) Functional interactions in bacteriorhodopsin: a theoretical analysis of retinal hydrogen bonding with water. Biophys J 68:25–39

Phatak P, Ghosh N, Yu H, Cui Q, Elstner M (2008) Amino acids with an intermolecular proton bond as proton storage site in bacteriorhodopsin. Proc Natl Acad Sci USA 105:19672–19677

Phatak P, Frähmke JS, Wanko M, Hoffmann M, Strudel P, Smith JC, Suhai S, Bondar AN, Elstner M (2009) Long-distance proton transfer with a break in the bacteriorhodopsin active site. J Am Chem Soc 131:7064–7078

Roux B, Nina M, Pomès R, Smith JC (1996) Thermodynamic stability of water molecules in the bacteriorhodopsin proton channel: a molecular dynamics free energy perturbation study. Biophys J 71:670–681

Royant A, Edman K, Ursby T, Pebay-Peyroula E, Landau EM, Neutze R (2000) Helix deformation is coupled to vectorial proton transport in the photocycle of bacteriorhodopsin. Nature 406:645–648

Sass H, Büldt G, Gessenich R, Hehn D, Neff D, Schlesinger R, Berendzen J, Ormos P (2000) Structural alterations for proton translocation in the M state of wild-type bacteriorhdopsin. Nature 406:649–653

Schobert B, Cupp-Vickery J, Hornak V, Smith SO, Lanyi JK (2002) Crystallographic structure of the K intermediate of bacteriorhodopsin: conservation of free energy after photoisomerization of the retinal. J Mol Biol 321:715–726

Singh UC, Kollman P (1986) A combined ab initio quantum mechanical and molecular mechanical method for carrying out simulations on complex molecular systems: applications to the $CH_3Cl + Cl^-$ exchange reaction and gas phase protonation of polyethers. J Comput Chem 7:718–730

Subramaniam S, Lindahl M, Bullough P, Faruki AR, Tittor J, Oesterhelt D, Brown L, Lanyi JK, Henderson R (1999) Protein conformational changes in the bacteriorhodopsin photocycle. J Mol Biol 287:145–161

Warshel A (1991) Computer modeling of chemical reactions in enzymes and solutions. John Wiley & Sons, New York

Wiener MC, White SH (1992) Structure of a fluid dioleoylphosphatidylcholine bilayer determined by joint refinement of x-ray

and neutron diffraction data. III. Complete structure. Biophys J 61:434–447

Zhou H, Tajkhorshid E, Frauenheim T, Suhai S, Elstner M (2002) Performance of the AM1, PM3, and SCC-DFTB methods in the study of conjugated Schiff base models. Chem Phys 277:91–103

Zscherp C, Schlesinger R, Tittor J, Oesterhelt D, Heberle J (1999) *In situ* determination of transient pKa changes of internal amino acids of bacteriorhodopsin by using time-resolved attenuated total reflection Fourier-transform infrared spectroscopy. Proc Natl Acad Sci USA 96:5498–5503